Precision frequency measurements of ^{3,4}He $2\,^3P \to 3\,^3D$ transitions at 588 nm

Pei-Ling Luo,[1] Jin-Long Peng,[2] Jinmeng Hu,[3] Yan Feng,[3] Li-Bang Wang,[1,4,*] and Jow-Tsong Shy[1,4,5,†]

[1]*Department of Physics, National Tsing Hua University, Hsinchu 30013, Taiwan*
[2]*Center for Measurement Standards, Industrial Technology Research Institute, Hsinchu 30011, Taiwan*
[3]*Shanghai Key Laboratory of Solid State Laser and Application and Shanghai Institute of Optics and Fine Mechanics, Chinese Academy of Sciences, Shanghai 201800, China*
[4]*Frontier Research Center on Fundamental and Applied Sciences of Matters, National Tsing Hua University, Hsinchu 30013, Taiwan*
[5]*Institute of Photonics Technologies, National Tsing Hua University, Hsinchu 30013, Taiwan*
(Received 4 November 2016; published 15 December 2016)

We report the frequency measurements of the $2\,^3P \to 3\,^3D$ transitions in ^{3,4}He at 588 nm using an optical frequency comb stabilized laser system. The Doppler-free spectra of the $2\,^3P \to 3\,^3D$ transitions are demonstrated in an rf discharged sealed-off helium cell using intermodulated fluorescence spectroscopy. The measured absolute frequency of the ^{4}He $2\,^3P_0 \to 3\,^3D_1$ transition is 510 059 755.352(28) MHz, which is more precise than the previous measurement by two orders of magnitude. The ionization energies of the ^{4}He $2\,^3P_0$ and $2\,^3S_1$ states can be derived from our result and agree very well with the previous experimental values. More importantly, the Lamb shift of the $2\,^3S_1$ state can be deduced to be 4057.086(34) MHz, which is two times more precise than the previous result. In addition, the absolute frequencies of the $2\,^3P_{0,1/2} \to 3\,^3D_{1,3/2}$, $2\,^3P_{0,1/2} \to 3\,^3D_{1,1/2}$, and $2\,^3P_{0,1/2} \to 3\,^3D_{2,3/2}$ transitions in ^{3}He are measured. Our precision surpasses the theoretical calculations by more than one to two orders of magnitude. The hyperfine separations of the $3\,^3D$ states in ^{3}He and the frequency differences between ^{4}He and ^{3}He transitions are also presented.

I. INTRODUCTION

Precision measurements and theoretical calculations of the low-lying states in atomic helium have played important roles in the development of the quantum electrodynamics (QED) of the two-electron atomic systems. Recently, the electronic structure of helium was calculated to high precision using few-body QED atomic models [1–4]. On the experimental side, thanks to the development of the optical frequency comb (OFC), high-precision measurements of several crucial helium transitions have been reported in recent years [5–11]. Comparisons among different experiments and theories yield valuable tests for the QED calculations. For instance, the ^{3}He-^{4}He isotope shifts in the $2\,^3S_1 \to 2\,^1S_0$ [5] and $2\,^3S \to 2\,^3P$ [6,7] transitions have been measured with a precision of a few kHz and the accurate difference in the nuclear charge radius has been determined. Nevertheless, a 4σ discrepancy of the ^{3}He-^{4}He nuclear charge radius difference has been found [12]. Furthermore, the absolute frequencies of the $2\,^1S_0 \to 2\,^1P_1$ [8,9], $2\,^1P_1 \to 3\,^1D_2$ [10], and $2\,^3S_1 \to 2\,^1P_1$ [11] transitions have been measured, yielding precise determinations of the ionization energies of the $2\,^1S_0$ and $2\,^1P_1$ states. The ionization energies of the $2\,^1P_1$ state in all recent experiments agree with each other, but disagree by over 3σ with the most accurate calculations [3]. In addition, although the determined ionization energies of helium $2\,^3S_1$ and $2\,^3P_J$ states are in moderate agreement with the theories, there is still a lack of accurate experimental determination and the current uncertainty of 60 kHz is mainly from the frequency measurement of the ^{4}He $2\,^3S_1 \to 3\,^3D_1$ two-photon transition [13]. Moreover, a discrepancy of 7.4σ between the theories

and experiments of the $3\,^1D$-$3\,^3D$ separation in ^{3}He needs to be resolved [1].

The spectral position of helium $2\,^3P \to 3\,^3D$ transitions is shown in Fig. 1. High-precision frequency measurements of helium $2\,^3P \to 3\,^3D$ transitions are essential to directly determine the ionization energy of the $2\,^3P$ state and investigate the fine structure and hyperfine intervals of the $2\,^3P$ and $3\,^3D$ states. Up to now, the only frequency metrology on $2\,^3P \to 3\,^3D$ transitions in ^{4}He was performed with an uncertainty of 2.7 MHz in 1984 [14]. Our preliminary spectral measurement of the ^{4}He $2\,^3P_{1,2} \to 3\,^3D_{1,2,3}$ transitions as well as their crossover lines has been presented using Doppler-free intermodulated fluorescence spectroscopy [15]. In this study, the $2\,^3P_0 \to 3\,^3D_1$ transition in ^{4}He and the $2\,^3P_{0,1/2} \to 3\,^3D_{1,3/2}$, $2\,^3P_{0,1/2} \to 3\,^3D_{1,1/2}$, and $2\,^3P_{0,1/2} \to 3\,^3D_{2,3/2}$ transitions in ^{3}He are chosen for absolute frequency measurements because the $2\,^3P_0$ state is approximately 30 GHz away from $2\,^3P_{1,2}$ states and the spectra are simpler. Furthermore, the previous determination of ^{4}He $2\,^3P_0$ ionization energy disagrees by about 3σ with the theoretical calculation [1].

In this work, the measured absolute frequency of the ^{4}He $2\,^3P_0 \to 3\,^3D_1$ transition has a relative uncertainty of 5×10^{-11}, which is two orders of magnitude more accurate than the previous measurement. The derived ionization energies of the ^{4}He $2\,^3P_0$ and $2\,^3S_1$ states are two times more precise than previous determinations. Furthermore, the absolute frequencies of $2\,^3P \to 3\,^3D$ transitions in ^{3}He are demonstrated. The hyperfine separations of $3\,^3D$ states and the frequency differences between ^{4}He and ^{3}He transitions are also reported.

II. EXPERIMENT

The schematic diagram of our experimental setup is shown in Fig. 2. The absolute frequency measurements of helium

_____

*lbwang@phys.nthu.edu.tw
†shy@phys.nthu.edu.tw
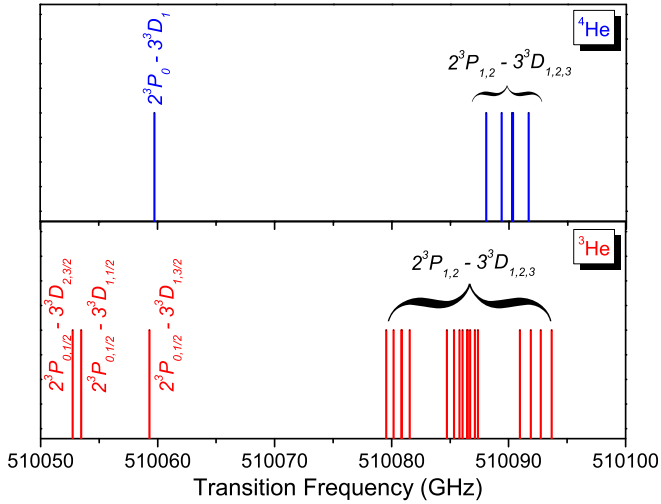
FIG. 1. The spectral position of helium $2\,^3P \to 3\,^3D$ transitions.

$2\,^3P \to 3\,^3D$ transitions at 588 nm are performed using a frequency-doubled Raman fiber amplifier boosted 1176 nm external cavity diode laser (ECDL) system [15] and an Er:fiber-based optical frequency comb (OFC) [16]. In order to accurately measure the spectrum, the ECDL is locked to a reference cavity with a finesse of 300 and a free spectral range of 500 MHz for frequency prestabilization. Then, the frequency of the ECDL is offset locked to one of the OFC lines and tuned by changing the repetition rate of the OFC. The repetition rate (f_r) and offset frequency (f_o) of the OFC are phase locked to frequency synthesizers referenced to a

calibrated cesium clock (Microsemi 5071A). The accuracy of our OFC is better than 1×10^{-12} at a 1000 sec integration time.

The spectral measurement of helium $2\,^3P \to 3\,^3D$ transitions is performed using Doppler-free intermodulated fluorescence technique [17]. The laser beam at 588 nm is generated by frequency doubling of a Raman fiber amplifier boosted 1176 nm ECDL using a MgO:PPLN crystal (HC Photonics). The laser power at 588 nm is stabilized using a liquid-crystal-based power stabilizer to reduce the power drift and fluctuation. Then, the laser beam is separated into two beams by a 50:50 beam splitter (BS) and sent to a 15-cm-long rf discharged helium cell. The cell is enclosed in a three-layer mu-metal box to reduce the earth magnetic field to <1 mG. The two beams are chopped at 559 and 399 Hz, respectively. The laser-induced fluorescence from the cell through a 586 nm fluorescence bandpass filter (bandwidth of 20 nm) was detected and demodulated by a lock-in amplifier at the sum frequency of 958 Hz.

In order to demonstrate precision measurements of the entire transition spectrum, the ECDL frequency is scanned step by step with an interval of approximately 2.55 MHz by tuning the repetition rate of the OFC. The signal at each frequency step is the average of the lock-in output in a recording time of 10 s. The used lock-in time constant is 100 ms and waiting time is 1 second after the change to the next frequency step. The optical frequency of the laser at 1176 nm is given by $f_L = n \times f_r + f_o - f_b$, where n is the mode number of the OFC and f_b is the beat frequency between ECDL and OFC at 1176 nm. Thus, the optical frequency at 588 nm is $2 \times f_L$.

III. RESULTS

Figure 3 shows a typical Doppler-free spectrum of the ^{4}He $2\,^3P_0 \to 3\,^3D_1$ transition. The measured spectrum is well fitted with the Lorentzian profile. The fitting residuals
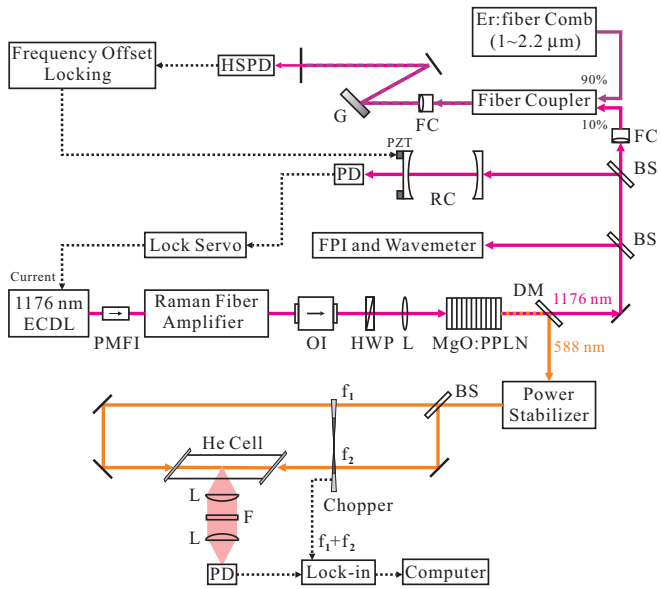

FIG. 2. Schematic diagram of the experimental setup. ECDL: external cavity diode laser; PMFI: polarization-maintaining fiber isolator; OI: optical isolator; HWP: half-wave plate; L: lens; PPLN: periodically poled LiNbO$_3$ crystal; DM: dichroic mirror; BS: beam splitter; F: filter; PD: photodiode; FPI: Fabry-Perot interferometer; RC: reference cavity; FC: fiber collimator; G: grating; HSPD: high-speed photodiode.
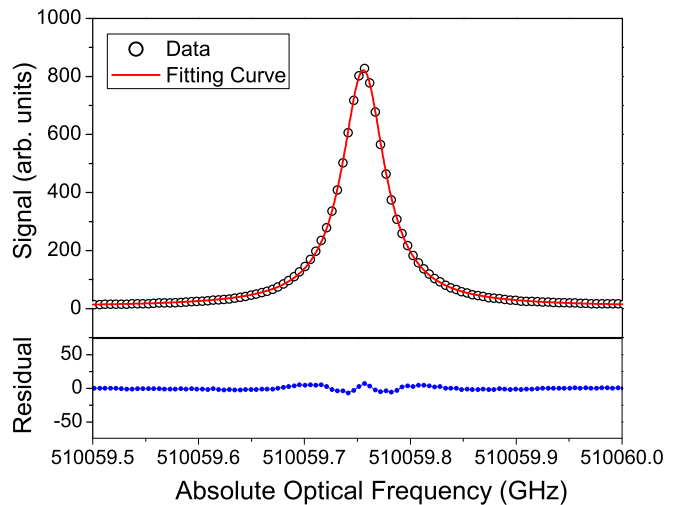

FIG. 3. A typical spectrum of the ^{4}He $2\,^3P_0 \to 3\,^3D_1$ transition. The experimental points are fitted with a Lorentzian profile. The bottom shows the fitting residuals. Here, the cell pressure is 200 mTorr. The total laser power is 11 mW and the rf discharge power is 22 W.
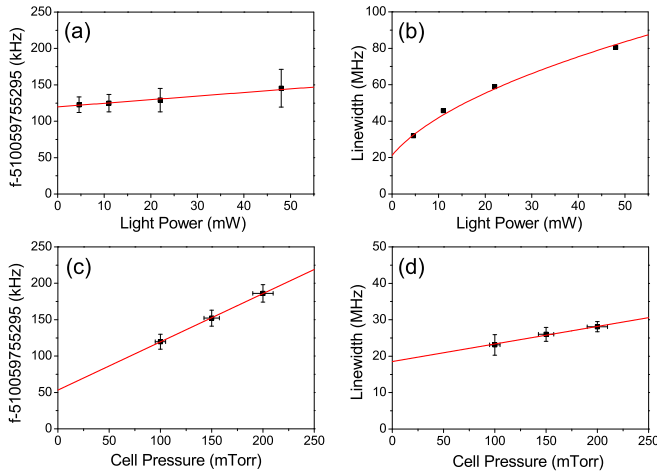
FIG. 4. The dependences of (a) the transition frequency and (b) the spectral linewidth on the total laser power. Here, the cell pressure is 100 mTorr. Each data point in (a) and (b) is obtained by a constant fit of 16 measurements. (c) Extrapolation of the transition frequency vs the cell pressure at zero light power. The coefficient of the pressure shift is 633(173) kHz/Torr. (d) Extrapolation of the spectral linewidth vs the cell pressure at zero light power. The coefficient of the pressure broadening is 48.2(4.8) MHz/Torr.

demonstrate that the measured spectrum has a symmetric line shape. We have scanned the laser frequency in both directions and found no differences in the line shape. In order to study the pressure shift and broadening, the Pyrex cells filled with pure ^{4}He at pressures of 100, 150, and 200 mTorr are used. The pressure uncertainty of each cell is estimated to be 5%. The center frequency and spectral linewidth are acquired by fitting the measured spectra in different experimental conditions. Figure 4 shows the dependences of the transition center frequency and the spectral linewidth of the ^{4}He $2\,^{3}P_0 \rightarrow 3\,^{3}D_1$ transition on the light power and cell pressure. In addition, the center frequency and spectral linewidth at different rf discharge power are also investigated. No significant variation of the center frequency and spectral linewidth are observed when the rf power is changed from 5 to 22 W. For each pressure, the center frequency and the spectral linewidth at zero light power are obtained by fitting the data versus the light power. Then, the linear extrapolation is used to determine the center frequency and the spectral linewidth at zero pressure. The obtained coefficients of the pressure shift and broadening are 633(173) kHz/Torr and 48.2(4.8) MHz/Torr respectively. The obtained linewidth at zero light power and pressure is 18.5(8) MHz, which is larger then the natural linewidth (11.2 MHz) due to broadening mechanisms in the discharge environment.

Table I lists the correction and uncertainty of the ^{4}He $2\,^{3}P_0 \rightarrow 3\,^{3}D_1$ transition frequency measurement from various sources. Taking the frequency shift and the statistical and systematical uncertainties into account, the absolute frequency of the ^{4}He $2\,^{3}P_0 \rightarrow 3\,^{3}D_1$ transition is determined to be 510 059 755.352(28) MHz. The experimental and theoretical values of the center frequency for the ^{4}He $2\,^{3}P_0 \rightarrow 3\,^{3}D_1$ transition are shown in Table II. Our result is more precise than the previous measurement [14] by two orders of magnitude. In addition, for the $2\,^{3}P_0 \rightarrow 3\,^{3}D_1$ transition

TABLE I. Correction and uncertainty budget of the ^{4}He $2\,^{3}P_0 \rightarrow 3\,^{3}D_1$ transition frequency measurement. Units are kHz.

Source	Shift	Uncertainty
Statistical error	0	26
OFC accuracy	0	2
Frequency locking of ECDL and OFC	0	2
Second-order Doppler shift	4	1
Zeeman effect	0	<1
Overall	4	28

frequency measurement, a discrepancy of 3.2σ (6.4 MHz) with the theoretical calculation [1] is presented. It should be an interesting result for the QED test in atomic helium.

More importantly, our measured ^{4}He $2\,^{3}P_0 \rightarrow 3\,^{3}D_1$ transition frequency can be used to determine the ionization energies of the $2\,^{3}P_0$ and $2\,^{3}S_1$ states. The comparisons of the ionization energies of the ^{4}He $2\,^{3}P_0$ and $2\,^{3}S_1$ states deduced from the experiments and QED calculations are shown in Figs. 5 and 6, respectively. The derived ionization energy of the ^{4}He $2\,^{3}P_0$ state is 876 078 648.322(34) MHz, given by our measured $2\,^{3}P_0 \rightarrow 3\,^{3}D_1$ transition frequency in this work and the theoretical ionization energy of the $3\,^{3}D_1$ state [1]. The derived ionization energy of the $2\,^{3}S_1$ state is 1 152 842 743.029(34) MHz, given by the derived ionization energy of the ^{4}He $2\,^{3}P_0$ state and the precisely measured frequency of the ^{4}He $2\,^{3}S_1 \rightarrow 2\,^{3}P_0$ transition [6]. The errors of the derived ionization energies of the ^{4}He $2\,^{3}P_0$ and $2\,^{3}S_1$ states include the uncertainties of the transition frequency measurements and 20 kHz error in the theoretical value of the $3\,^{3}D_1$ ionization energy [1]. Our results of the ^{4}He $2\,^{3}P_0$ and $2\,^{3}S_1$ ionization energies agree with the previous values obtained by the frequency measurements of the $2\,^{3}S_1 \rightarrow 3\,^{3}D_1$ two-photon transition [13] and the $2\,^{3}S_1 \rightarrow 2\,^{3}P_0$ transition [6] and the precision of this work is successfully improved by a factor of 2. Moreover, the Lamb shift of the $2\,^{3}S_1$ state can be deduced to be 4057.086(34) MHz, which is two times more precise than the previous determination [13] and it can be compared with the current theoretical prediction [4058.8(2.5) MHz]. On the other hand, although the experiments are in reasonable agreement with theories, all experimental values of

TABLE II. Experimental and theoretical values for the $2\,^{3}P_0 \rightarrow 3\,^{3}D_1$ transition in ^{4}He and the $2\,^{3}P_{0,1/2} \rightarrow 3\,^{3}D_{1,3/2}$, $2\,^{3}P_{0,1/2} \rightarrow 3\,^{3}D_{1,1/2}$, and $2\,^{3}P_{0,1/2} \rightarrow 3\,^{3}D_{2,3/2}$ transitions in ^{3}He.

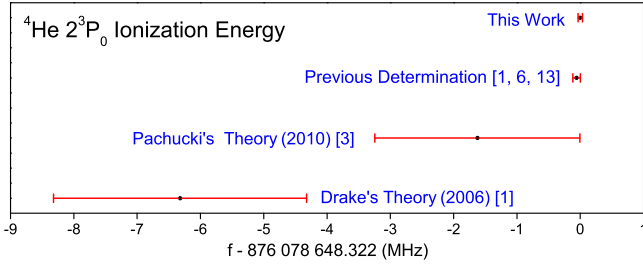| Transition	Center frequency (MHz)
^{4}He $2\,^{3}P_0 \rightarrow 3\,^{3}D_1$	510 059 755.352(28) (this work)
	510 059 755.4(2.7) [14]
	510 059 749.0(2.0) [1]
	510 059 753.7(1.6) [3]
^{3}He $2\,^{3}P_{0,1/2} \rightarrow 3\,^{3}D_{1,3/2}$	510 059 290.494(61) (this work)
	510 059 284.1(2.0) [1]
^{3}He $2\,^{3}P_{0,1/2} \rightarrow 3\,^{3}D_{1,1/2}$	510 053 456.421(123) (this work)
	510 053 450.1(2.0) [1]
^{3}He $2\,^{3}P_{0,1/2} \rightarrow 3\,^{3}D_{2,3/2}$	510 052 734.035(137) (this work)
	510 052 727.7(2.0) [1]

FIG. 5. Comparison of the ionization energy of the ^{4}He $2\,^3P_0$ state deduced from the experimental determinations and QED calculations.

the ionization energies are higher than the theoretical values. Besides, the ionization energies in the singlet low-lying states, such as $1\,^1S_0$, $2\,^1S_0$, and $2\,^1P_1$ states, also show a similar trend [10,18].

The absolute frequency measurements of the ^{3}He $2\,^3P \rightarrow 3\,^3D$ transitions are performed using the same experimental scheme. Figure 7(a) shows a typical Doppler-free spectrum of the ^{3}He $2\,^3P_{0,1/2} \rightarrow 3\,^3D_{1,3/2}$ transition. Since this transition is well isolated, the spectrum can be fitted using the Lorentzian profile. In addition, a typical spectra of the ^{3}He $2\,^3P_{0,1/2} \rightarrow 3\,^3D_{1,1/2}$ and $2\,^3P_{0,1/2} \rightarrow 3\,^3D_{2,3/2}$ transitions including the crossover line, shown in Fig. 7(b), are fitted with a summation of three Lorentzian peaks, given by $S = L(\nu\text{-}\nu_1) + L(\nu\text{-}\nu_2) + L(\nu\text{-}\nu_3)$, where ν_1 and ν_3 are the center frequencies of the ^{3}He $2\,^3P_{0,1/2} \rightarrow 3\,^3D_{1,1/2}$ and $2\,^3P_{0,1/2} \rightarrow 3\,^3D_{2,3/2}$ transitions, respectively, and ν_2 is $(\nu_1 + \nu_3)/2$. The fitting residuals demonstrate that the measured spectra of each transition have symmetric line shapes.

The center frequency and spectral linewidth of the ^{3}He $2\,^3P \rightarrow 3\,^3D$ transitions at different experimental conditions, such as different gas pressures, light powers, and discharge powers, are investigated and analyzed. Furthermore, in order to investigate the line shift due to the quantum mechanical interference effect [19,20], we have also changed the location and orientation of the detector and the polarization of laser beams, but no significant variation of the line center can be found. Therefore, we conclude that the line center is not affected significantly by the quantum mechanical interference in our case. The measured absolute frequencies and theoretical values for the $2\,^3P_{0,1/2} \rightarrow 3\,^3D_{1,3/2}$, $2\,^3P_{0,1/2} \rightarrow 3\,^3D_{1,1/2}$, and $2\,^3P_{0,1/2} \rightarrow 3\,^3D_{2,3/2}$ transitions in ^{3}He are listed in Table II. Compared with our measured ^{4}He $2\,^3P_0 \rightarrow 3\,^3D_1$ transition, the signal-to-noise ratio (SNR) of the ^{3}He transitions are
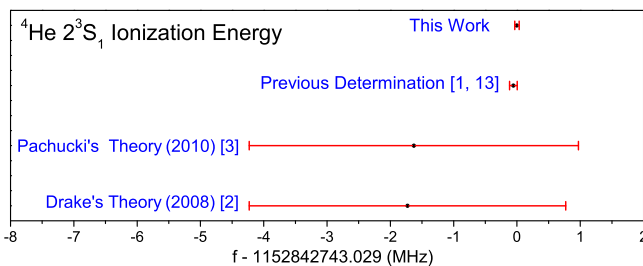

FIG. 6. Comparison of the ionization energy of the ^{4}He $2\,^3S_1$ state deduced from the experimental determinations and QED calculations.
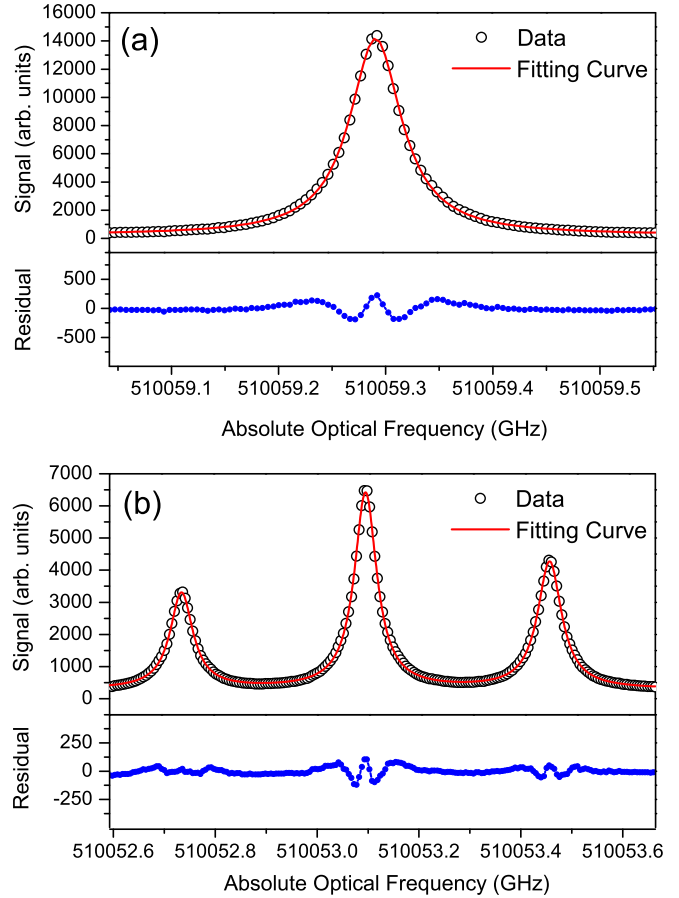

FIG. 7. (a) A typical spectrum of the ^{3}He $2\,^3P_{0,1/2} \rightarrow 3\,^3D_{1,3/2}$ transition. The experimental points are fitted with a Lorentzian profile. The bottom shows the fitting residuals. Here, the cell pressure is 200 mTorr. The total laser power is 22 mW and the rf discharge power is 22 W. (b) Typical spectra of the ^{3}He $2\,^3P_{0,1/2} \rightarrow 3\,^3D_{2,3/2}$ (left) and $2\,^3P_{0,1/2} \rightarrow 3\,^3D_{1,1/2}$ (right) transitions as well as their crossover line (center). The experimental points are fitted with three Lorentzian peaks. The bottom shows the fitting residuals. Here, the cell pressure is 150 mTorr. The total laser power is 48 mW and the rf discharge power is 22 W.

2–3 times lower. As a result, the uncertainties of the center frequency for ^{3}He transitions are 2–3 times worse. Nevertheless, the precision of our results still surpasses the theoretical calculations by more than one to two orders of magnitude. The determined $3\,^3D$ hyperfine separations in ^{3}He agree with the theoretical calculations, as shown in Table III. Besides, the frequency differences between the ^{4}He $2\,^3P_0 \rightarrow 3\,^3D_1$ and the ^{3}He $2\,^3P \rightarrow 3\,^3D$ transitions are shown in Table IV. Our results are comparable with the theoretical values, given by

TABLE III. Experimental and theoretical values for the $3\,^3D$ hyperfine separations in ^{3}He.

Hyperfine separations	This work (MHz)	Theory (MHz) [1]
$3\,^3D_{1,3/2}$-$3\,^3D_{1,1/2}$	5834.073(137)	5834.03(4)
$3\,^3D_{1,3/2}$-$3\,^3D_{2,3/2}$	6556.459(150)	6556.42(3)
$3\,^3D_{1,1/2}$-$3\,^3D_{2,3/2}$	722.386(184)	722.39(4)

TABLE IV. Frequency differences between the ^{4}He $2\,^3P_0 \to 3\,^3D_1$ transition and the ^{3}He $2\,^3P \to 3\,^3D$ transitions.

Transitions in ^{3}He	This work (MHz)	Theory (MHz) [1]
$2\,^3P_{0,1/2} \to 3\,^3D_{1,3/2}$	464.858(67)	464.974(14)
$2\,^3P_{0,1/2} \to 3\,^3D_{1,1/2}$	6298.931(126)	6299.006(35)
$2\,^3P_{0,1/2} \to 3\,^3D_{2,3/2}$	7021.317(140)	7021.397(25)

the theoretical isotope shift and the calculated hyperfine shifts [1]. Our results should be helpful for testing the theoretical calculations in ^{3}He.

IV. CONCLUSIONS

In conclusion, the precision frequency measurements of the $2\,^3P_0 \to 3\,^3D_1$ transition in ^{4}He as well as the $2\,^3P_{0,1/2} \to 3\,^3D_{1,3/2}$, $2\,^3P_{0,1/2} \to 3\,^3D_{1,1/2}$, and $2\,^3P_{0,1/2} \to 3\,^3D_{2,3/2}$ transitions in ^{3}He have been achieved. The measured transition frequencies are one to two orders of magnitude more precise than current best theoretical calculations and are in reasonable agreement with the calculated values. Our results yield the

independent determinations of the ionization energies of the ^{4}He $2\,^3P_0$ and $2\,^3S_1$ state and provide crucial tests of QED calculations in helium low-lying states. More importantly, the deduced Lamb shift of the $2\,^3S_1$ state is two times more precise than the previous result. Recently, we have succeeded in the observation of the Doppler-free spectra of the spin-forbidden $2\,^3P \to 3\,^1D$ transitions [15]. We anticipate that the discrepancy of the ^{3}He $3\,^1D$-$3\,^3D$ separations between the theories and experiment [1] will be resolved after we perform the frequency measurements of the spin-forbidden $2\,^3P \to 3\,^1D$ transitions.

[1] D. C. Morton, Q. Wu, and G. W. F. Drake, Can. J. Phys. **84**, 83 (2006).

[2] G. W. F. Drake and Z.-C. Yan, Can. J. Phys. **86**, 45 (2008).

[3] V. A. Yerokhin and K. Pachucki, Phys. Rev. A. **81**, 022507 (2010).

[4] P.-P. Zhang, Z.-X. Zhong, C.-Z. Yan, and T.-Y. Shi, Chin. Phys. B **24**, 033101 (2015).

[5] R. van Rooij, J. S. Borbely, J. Simonet, M. D. Hoogerland, K. S. E. Eikema, R. A. Rozendaal, and W. Vassen, Science **333**, 196 (2011).

[6] P. C. Pastor, G. Giusfredi, P. DeNatale, G. Hagel, C. de Mauro, and M. Inguscio, Phys. Rev. Lett. **92**, 023001 (2004).

[7] P. CancioPastor, L. Consolino, G. Giusfredi, P. DeNatale, M. Inguscio, V. A. Yerokhin, and K. Pachucki, Phys. Rev. Lett. **108**, 143001 (2012).

[8] P.-L. Luo, J.-L. Peng, J.-T. Shy, and L.-B. Wang, Phys. Rev. Lett. **111**, 013002 (2013).

[9] P.-L. Luo, J.-L. Peng, J.-T. Shy, and L.-B. Wang, Phys. Rev. Lett. **111**, 179901(E) (2013).

[10] P.-L. Luo, Y.-C. Guan, J.-L. Peng, J.-T. Shy, and L.-B. Wang, Phys. Rev. A **88**, 054501 (2013).

[11] R. P. M. J. W. Notermans and W. Vassen, Phys. Rev. Lett. **112**, 253002 (2014).

[12] K. Pachucki and V. A. Yerokhin, J. Phys. Chem. Ref. Data **44**, 031206 (2015).

[13] C. Dorrer, F. Nez, B. de Beauvoir, L. Julien, and F. Biraben, Phys. Rev. Lett. **78**, 3658 (1997).

[14] C. J. Sansonetti and W. C. Martin, Phys. Rev. A **29**, 159 (1984).

[15] P.-L. Luo, J. Hu, Y. Feng, L.-B. Wang, and J.-T. Shy, Appl. Phys. B **120**, 279 (2015).

[16] J.-L. Peng, H. Ahn, R.-H. Shu, H.-C. Chui, and J. Nicholson, Appl. Phys. B **86**, 49 (2007).

[17] M. Sorem and A. Shawlow, Opt. Commun. **5**, 148 (1972).

[18] D. Z. Kandula, C. Gohle, T. J. Pinkert, W. Ubachs, and K. S. E. Eikema, Phys. Rev. A **84**, 062512 (2011).

[19] A. Marsman, M. Horbatsch, and E. A. Hessels, Phys. Rev. A **91**, 062506 (2015).

[20] A. Marsman, E. A. Hessels, and M. Horbatsch, Phys. Rev. A **89**, 043403 (2014).